Systematics of magnetic dipole strength in the stable even-mass Mo isotopes

G. Rusev,[1,2] R. Schwengner,[1] F. Dönau,[1] M. Erhard,[1] S. Frauendorf,[1,3] E. Grosse,[1] A. R. Junghans,[1] L. Käubler,[1] K. Kosev,[1] L. K. Kostov,[2] S. Mallion,[1] K. D. Schilling,[1] A. Wagner,[1] H. von Garrel,[4] U. Kneissl,[4] C. Kohstall,[4,*] M. Kreutz,[4] H. H. Pitz,[4] M. Scheck,[4,†] F. Stedile,[4] P. von Brentano,[5] C. Fransen,[5] J. Jolie,[5] A. Linnemann,[5] N. Pietralla,[5,6] and V. Werner[5,7]

[1]*Institut für Kern- und Hadronenphysik, Forschungszentrum Rossendorf, D-01314 Dresden, Germany*

[2]*Institute for Nuclear Research and Nuclear Energy, BAS, BG-1784 Sofia, Bulgaria*

[3]*Department of Physics, University of Notre Dame, Notre Dame, Indiana 46556, USA*

[4]*Institut für Strahlenphysik, Universität Stuttgart, D-70569 Stuttgart, Germany*

[5]*Institut für Kernphysik, Universität Köln, D-50937 Köln, Germany*

[6]*Nuclear Structure Laboratory, Department of Physics and Astronomy, SUNY, Stony Brook, New York 11794-3800, USA*

[7]*Wright Nuclear Structure Laboratory, Yale University, New Haven, Connecticut 06520-8124, USA*

(Received 1 February 2006; published 12 April 2006)

The nuclides ^{92}Mo, ^{98}Mo, and ^{100}Mo have been studied in photon-scattering experiments by using bremsstrahlung produced at an electron energy of 6 MeV at the ELBE accelerator of the Forschungszentrum Rossendorf and at electron energies from 3.2 to 3.8 MeV at the Dynamitron accelerator at the University of Stuttgart. Six dipole transitions in ^{98}Mo and 19 in ^{100}Mo were observed for the first time in the energy range from 2 to 4 MeV. The experimental results are compared with predictions of the shell model and with predictions of the quasiparticle random-phase approximation (QRPA) in a deformed basis. The latter show significant contributions of isovector-orbital and isovector-spin vibrations. The change of the magnetic dipole strength in the isotopic chain of the even-mass isotopes from ^{92}Mo to ^{100}Mo is discussed. The calculations within the QRPA are extrapolated to the particle-separation energies to estimate the possible influence of $M1$ strength on the stability of the nuclides against photodissociation in cosmic scenarios.

DOI: 10.1103/PhysRevC.73.044308 PACS number(s): 21.60.Jz, 23.20.Lv, 25.20.Dc, 27.60.+j

I. INTRODUCTION

The origin and the strength of the magnetic dipole ($M1$) radiation emitted from excited nuclear states has been the subject of various experimental and theoretical investigations. In even-even nuclei, there are basically two sources for the generation of $M1$ radiation [1]. Firstly, based on large nucleonic g factors, considerable $M1$ strength can be produced by spin-flip transitions arising from particle excitations between spin-orbit partner states with $j = l \pm 1/2$. This spin-magnetic strength splits into several peaks [2,3] around an energy corresponding to the spacing between the partner orbits, and it was found to be quenched in heavy nuclei [4]. Secondly, substantial $M1$ strength can be formed in deformed nuclei by orbital-magnetic transitions between states in which high-j proton and high-j neutron orbits are reoriented. According to this possibility, the existence of a particular isovector excitation with spin and parity 1^+ was predicted within a semiclassical two-rotor model [5] and first observed a few years later in electron-scattering experiments [6]. This so-called scissors mode is caused by a rotational oscillation of the neutron system against the proton system which manifests as a group of 1^+ states around 3 MeV with a summed transition strength of up to $\sum B(M1, 0^+ \rightarrow 1^+) \approx 3\,\mu_N^2$. Such 1^+ states have been studied systematically in numerous photon-scattering experiments on rare-earth nuclei. Overviews of these experiments are given, e.g., in Refs. [7,8]. The summed $M1$ strength of the 1^+ states was found to be proportional to the square of the quadrupole deformation [9,10], which could be understood on the basis of a phenomenological sum-rule approach [11]. In contrast to the scissors interpretation, the 1^+ states in deformed nuclei were alternatively described as isovector-spin excitations in terms of a microscopic random-phase approximation (RPA) model [12].

In spherical nuclei, a different mechanism has been proposed to explain the appearance of low-lying 1^+ states. Thus, in the nearly spherical nucleus ^{94}Mo, the first 1^+ state with a value of $B(M1, 0^+ \rightarrow 1^+) = 0.48(3)\,\mu_N^2$ was described within the proton-neutron version of the interacting-boson model (IBM-2) as a two-phonon state resulting from the coupling of the first 2^+ state with another 2^+ state of mixed proton-neutron symmetry [13,14]. Alternatively, this state can be explained in the framework of the shell model as an excitation with the two-proton-two-neutron configuration $\pi(0g_{9/2}^2)\nu(1d_{5/2}^2)$ [15]. Similarly, the 1^+ states found in the nearly spherical neighbor ^{96}Mo were considered as fragments of the 1^+ member of two-phonon multiplets [16].

For the investigation of the behavior of the $M1$ strength with increasing neutron number and developing nuclear deformation, the chain of stable even-even Mo isotopes with $A = 92$–100 provides a favorable example. While the lightest isotope ^{92}Mo with $N = 50$ has a spherical shape, the heaviest isotopes ^{98}Mo and ^{100}Mo display a moderate quadrupole deformation around $\varepsilon_2 \approx 0.2$, as was shown for $A = 100$ in the framework of the Hartree-Fock-Bogoliubov model [17–19], where the deformation is caused by polarization effects resulting from the strong proton-neutron interaction.

*Present address: Phywe Systeme, D-37079 Göttingen, Germany.

†Present address: Department of Chemistry and Physics & Astronomy, University of Kentucky, Lexington, Kentucky 40506-0055, USA.

The shapes of the considered Mo isotopes are soft, moreover, the coexistence of different shapes shows up in the occurrence of low-lying excited 0^+ states as recently studied by means of Coulomb excitation for ^{98}Mo [20] and ^{96,100}Mo [21].

In the photon-scattering experiments described in the following, we observed transitions in ^{98}Mo and ^{100}Mo that deexcite states with spin $J = 1$ at excitation energies around 3.5 MeV to the 0^+ ground states as well as to the first excited 0^+ states. In a preceding paper, we developed a model that considers the $J = 1$ states as one-particle-one-hole excitations and allowed us to derive the mixing coefficients of the two mixed 0_1^+ and 0_2^+ states from the transition intensities measured in these experiments [22].

The present work focuses on the experimental $M1$ strength distributions up to excitation energies of about 4 MeV in ^{92}Mo, ^{98}Mo, and ^{100}Mo. We complement the present results with data obtained in previous work for ^{94}Mo [13,14] and ^{96}Mo [16] in order to discuss the evolution of the $M1$ strength in the chain of Mo isotopes.

II. EXPERIMENTAL METHODS AND RESULTS

Photon scattering, frequently called nuclear-resonance-fluorescence (NRF), provides a sensitive probe for the excitation of states with dominantly spin $J = 1$ and possibly $J = 2$ in even-even nuclei, and allows the determination of level lifetimes in the order of 10^{-15} s (see, e.g., Ref. [8]). In the present experiments, bremsstrahlung produced during the deceleration of electrons in a radiation converter was used to excite states in the nuclide under investigation and simultaneously states in the nuclides ^{11}B [23], ^{13}C [24], and ^{27}Al [25] which have known scattering cross sections and were used as calibration standards for the determination of the photon flux. The integrated scattering cross section of an observed level is calculated relative to those for levels of the calibration standard $\sigma_s(E_x^{\mathrm{cal}})$,

$$\sigma_s(E_x) = \sigma_s\left(E_x^{\mathrm{cal}}\right)\frac{I_\gamma(E_\gamma,\theta)}{I_\gamma\left(E_\gamma^{\mathrm{cal}},\theta\right)}\frac{W\left(E_\gamma^{\mathrm{cal}},\theta\right)}{W(E_\gamma,\theta)}\frac{N^{\mathrm{cal}}}{N}\frac{\Phi\left(E_\gamma^{\mathrm{cal}}\right)}{\Phi(E_\gamma)}, \tag{1}$$

where $I_\gamma(E_\gamma,\theta)$ denotes the intensity of a considered ground-state transition at E_γ and at an angle θ relative to the incident beam, $W(E_\gamma,\theta)$ is the angular correlation of this transition, N the number of atoms in the sample, and $\Phi(E_\gamma)$ the relative photon flux at E_x. The quantities with the superscript "cal" correspond to the calibration standard. The widths of the levels are calculated using the relation

$$\sigma_s(E_x) = \left(\frac{\pi\hbar c}{E_x}\right)^2\frac{2J_x+1}{2J_0+1}\frac{\Gamma_0^2}{\Gamma}, \tag{2}$$

where E_x, J_x, and Γ denote energy, spin, and total width of the excited level. The quantities J_0 and Γ_0 represent the spin of the ground state and the partial width of the transition to the ground state. The multipole order of an observed transition at E_γ is determined by comparing the ratio $I_\gamma(E_\gamma, 90^\circ)/I_\gamma(E_\gamma, 127^\circ)$ of the γ-ray intensities observed at 90° and 127° with the expected values of 0.73 and 2.28 for dipole and quadrupole transitions in even-even nuclei, respectively, which take into account the opening angle of the detectors in the present experiments. A definite assignment of the multipole order of the transitions was made if one theoretical intensity ratio was within two standard deviations of the measured value and the alternative was excluded by at least three standard deviations. Parities of states are suggested by the so-called Alaga rules for the ratios of the strengths of transitions deexciting a $J = 1$, $K = 0$ state or a $J = 1$, $K = 1$ state to the 2^+ and to the ground state in a deformed nucleus [26], that is,

$$\begin{aligned}\frac{B(1, K=0)\rightarrow 2^+)}{B(1, K=0)\rightarrow 0^+)} &= 2,\\ \frac{B(1, K=1)\rightarrow 2^+)}{B(1, K=1)\rightarrow 0^+)} &= 0.5,\end{aligned} \tag{3}$$

in conjunction with the fact that 1^- states have $K = 0$ and 1^+ states have $K = 1$ [27,28]. The reduced transition strengths $B(E1)$, $B(M1)$, and $B(E2)$ are proportional to the partial width Γ_0:

$$B(E1)\uparrow = \frac{2J_x+1}{2J_0+1}B(E1)\downarrow = 2.866\times 10^{-3}\frac{\Gamma_0}{E_\gamma^3}\,e^2\ \mathrm{fm}^2, \tag{4}$$

$$B(M1)\uparrow = \frac{2J_x+1}{2J_0+1}B(M1)\downarrow = 0.2598\frac{\Gamma_0}{E_\gamma^3}\,\mu_N^2, \tag{5}$$

$$B(E2)\uparrow = \frac{2J_x+1}{2J_0+1}B(E2)\downarrow = 6201\frac{\Gamma_0}{E_\gamma^5}\,e^2\ \mathrm{fm}^4, \tag{6}$$

where Γ_0 is taken in meV and E_γ in MeV [8].

Detection limits corresponding to the minimum detected peak area P were determined according to the relation [29]

$$P = 1.65\sqrt{2B}, \tag{7}$$

where B is the integrated area of the background in an energy interval with the width of two times the typical full width at half maximum of the observed peaks at the same energy, and the factor 1.65 corresponds to a 95% confidence limit. A minimum value of the ground-state width Γ_0 is calculated from P and Eq. (1) under the assumption that $J_x = 1$. We apply the detection limits to prove whether a peak can be accepted as a transition.

A. Photon-scattering experiment on ^{92}Mo

The low-lying excitations in ^{92}Mo were investigated at the new bremsstrahlung facility [30] at the superconducting electron accelerator ELBE of the Forschungszentrum Rossendorf. The bremsstrahlung was produced by irradiation of a 4 μm thick niobium radiator with a continuous-wave electron beam of a kinetic energy of 6.0 MeV and an average current of 300 μA. A narrow photon beam was formed by a 2.6 m long aluminium collimator with an aperture of 2.5 mrad placed in a heavy concrete wall. For background reduction, the target was placed in an evacuated beam pipe and the photon beam was absorbed in a photon-beam dump after passing the target. The target consisted of 2036 mg ^{92}Mo with an enrichment of 97.31%. The molybdenum target was combined with ^{11}B enriched to 99.52% with a mass of 456 mg for the calibration of

TABLE I. γ rays assigned to ^{92}Mo, ^{98}Mo, and ^{100}Mo.

E_x[a] keV	E_γ keV	J_x	J_f	b_f[b] %	$\frac{I_\gamma(90^\circ)}{I_\gamma(127^\circ)}$[c]	σ_s[d] eV b	Γ[e] MeV	$B(E1)\uparrow$[f] $10^{-3}e^2$ fm^2	$B(M1)\uparrow$[f] $10^{-3}\,\mu_N^2$	$B(E2)\uparrow$[f] e^2 fm^4
^{92}Mo										
1509.8(1)[g]	1509.8(1)	2^+	0^+							
3091.4(2)	3091.3(2)	2^{+}[h]	0^+	82(2)[i]	1.9(5)	27(3)	20(3)			362(44)
3925.8(2)	3925.7(2)	2^{+}[h]	0^+	65(5)[i]	1.9(7)	22(4)	42(8)			183(33)
3944.0(2)	3943.9(2)	1	0^+	100[i]	1.0(2)	27(3)	36(5)	1.7(2)	153(19)	
4494.8(6)	4494.7(6)	2^{+}[h]	0^+	100[i]		8.2(14)	8.7(15)			29(5)
4633.7(1)	4633.6(1)	$1^{(-)}$[h]	0^+	59(19)[i]	0.72(7)	43(3)	231(106)	3.93(13)	356(117)	
^{98}Mo										
3257.8(1)	3257.8(1)	1	0^+	100	0.71(8)	4.5(4)	4.1(3)	0.34(3)	31(3)	
3405.0(1)	3405.0(1)	1	0^+	100	0.68(3)	44(3)	44(3)	3.2(2)	289(19)	
3457.1(1)	3457.0(1)	1	0^+	100	0.70(3)	34(2)	35(2)	2.45(16)	222(15)	
3551.2(1)	3551.2(1)	1	0^+	87.7(14)	0.78(8)	28(2)	35(3)	0.65(6)[j]	58(6)[j]	
	2816.9(2)	1	0_2^+	12.3(14)	0.71(19)			0.18(4)[j]	17(3)[j]	
3703.9(2)	3703.9(2)	1	0^+	100	0.72(18)	3.5(5)	4.2(6)	0.23(3)	21(3)	
^{100}Mo										
2633.3(1)	2633.2(1)	1	0^+	100	0.6(3)	1.5(3)	0.90(18)	0.14(3)	13(3)	
2901.2(1)	2901.2(1)	1	0^+	100	0.73(20)	2.0(2)	1.43(17)	0.17(2)	15.2(18)	
2906.4(1)	2906.3(1)	1	0^+	100	0.95(19)	1.70(18)	1.25(13)	0.15(2)	13.2(14)	
3065.9(1)	3065.9(1)	1	0^+	100	0.62(9)	2.8(3)	2.2(2)	0.22(2)	20.2(19)	
3199.0(2)	3199.0(2)	1	0^+	100	0.66(17)	2.2(3)	2.0(3)	0.17(2)	15.7(20)	
3242.5(1)	3242.5(1)	1	0^+	100	0.70(10)	3.6(4)	3.3(4)	0.28(3)	25(3)	
3290.1(1)	3290.1(1)	$1^{(+)}$[k]	0^+	70(4)	0.72(7)	7.6(6)	10.7(15)	0.20(4)[j]	18(4)[j]	
	2754.7(2)	$1^{(+)}$[k]	2_1^+	15(3)	0.79(19)			0.07(3)[j]	7(2)[j]	
	2595.2(1)	$1^{(+)}$[k]	0_2^+	15(4)	0.74(20)			0.09(3)[j]	8(3)[j]	
3342.1(1)	3342.0(1)	1	0^+	100	0.69(13)	2.7(3)	2.6(3)	0.20(2)	18(2)	
3483.4(1)	3483.4(1)	$1^{(+)}$[k]	0^+	80.9(16)	0.68(7)	43(3)	55(5)	1.02(12)[j]	91(10)[j]	
	2948.2(1)	$1^{(+)}$[k]	2_1^+	10(1)	0.72(13)			0.21(4)[j]	18(3)[j]	
	2419.8(1)	$1^{(+)}$[k]	2_2^+	9(1)	0.62(12)			0.34(7)[j]	31(6)[j]	
3570.3(1)	3570.3(1)	1	0^+	100	0.75(10)	21.9(18)	24.2(19)	1.52(12)	138(11)	
3599.9(2)	3599.8(2)	1	0^+	100	1.0(4)	2.3(4)	2.5(4)	0.16(2)	14(2)	
3614.8(1)	3614.7(1)	1	0^+	100	0.64(15)	7.3(7)	8.2(8)	0.50(5)	45(5)	
3627.9(1)	3627.8(1)	1	0^+	100	0.71(12)	12.6(12)	14.4(14)	0.86(8)	78(8)	
3658.8(1)	3658.7(1)	$1^{(+)}$[k]	0^+	83(4)	0.65(14)	20.7(19)	25(4)	0.41(8)[j]	36(7)[j]	
	2595.2(1)	$1^{(+)}$[k]	2_2^+	17(4)	0.74(20)			0.23(9)[j]	20(8)[j]	

[a]Level energy. This value is recoil and Doppler-shift corrected.
[b]Branching ratio $b_f = \Gamma_f/\Gamma$.
[c]Ratio of γ-ray intensities observed at 90° and 127° relative to the incident beam.
[d]Integrated scattering cross section.
[e]Total width $\Gamma = \Gamma_0/b_0$.
[f]Reduced transition strength.
[g]Scattering cross section and width of this level are not given, since it may be fed from higher-lying levels.
[h]Parity taken from Ref. [33].
[i]Branching ratio taken from Ref. [32].
[j]Reduced transition strengths $B(E1)\downarrow$ or $B(M1)\downarrow$.
[k]Parity assigned according to the Alaga rules.

the photon flux. The relative photon flux determined from the ^{11}B transitions was interpolated by using the approximation of the bremsstrahlung spectrum given in Ref. [31]. γ rays scattered from the target were measured with four high-purity germanium (HPGe) detectors of 100% efficiency relative to a 3×3 in^2 NaI detector, two of them placed at 90° and the other two at 127° relative to the incident photon beam. All detectors were equipped with escape-suppression shields made of bismuth germanate (BGO) scintillation detectors with thicknesses of 3 cm. Spectra of scattered photons measured at 127° and 90° for 72 h are shown in Fig. 1. Six transitions were observed in ^{92}Mo, which are listed in Table I. The results for the levels at 3091.4, 3925.8, 3944.0, and 4633.7 keV are consistent with the ones obtained in previous work [32]. In addition, we observed a transition at 4494.7 keV in the spectrum measured at 90°, and we tentatively assign $J = (2)$

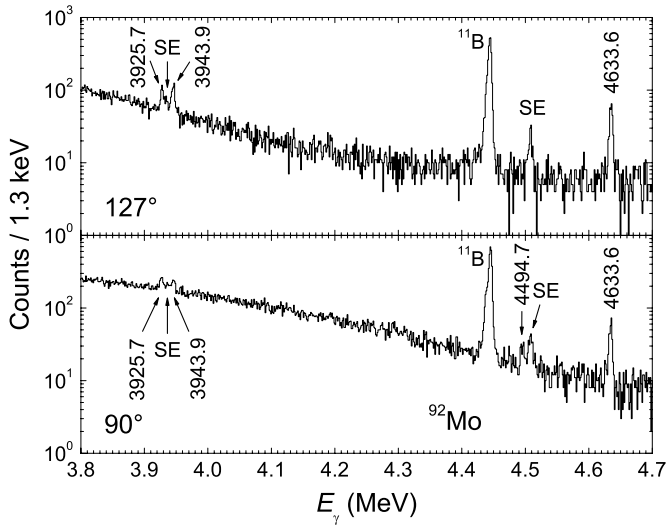

FIG. 1. Spectra of photons scattered from ^{92}Mo, measured at 127° (top) and at 90° (bottom) relative to the beam and at an electron energy of 6 MeV. Peaks labeled with their energies in keV correspond to transitions assigned to ^{92}Mo. SE marks single-escape peaks.

to the corresponding level. A level at 4493.9 keV had also been observed in electron-scattering experiments [33] with an assignment of $J^\pi = 2^+$. We cannot confirm additional levels proposed on the basis of previous photon-scattering experiments at $E_e = 8$ and 10 MeV [33,34] and assume that the corresponding γ rays are transitions from levels with energies greater than 6 MeV to low-lying levels.

The ratios $I_\gamma(E_\gamma, 90°)/I_\gamma(E_\gamma, 127°)$ and a comparison of the partial widths with the detection limits are presented in Fig. 2. A level scheme of ^{92}Mo as deduced from the present experiment is shown in Fig. 3.

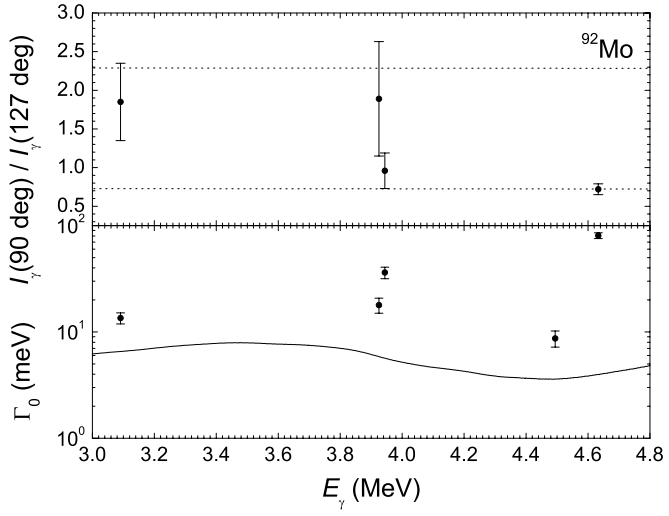

FIG. 2. Top: Ratios $I_\gamma(90°)/I_\gamma(127°)$ for transitions in ^{92}Mo, with the expected values for dipole (0.73) and quadrupole (2.28) transitions shown as dotted lines. Bottom: Partial widths of the ground-state transitions (filled circles) and the detection limits obtained for the spectrum at 127° (solid line).

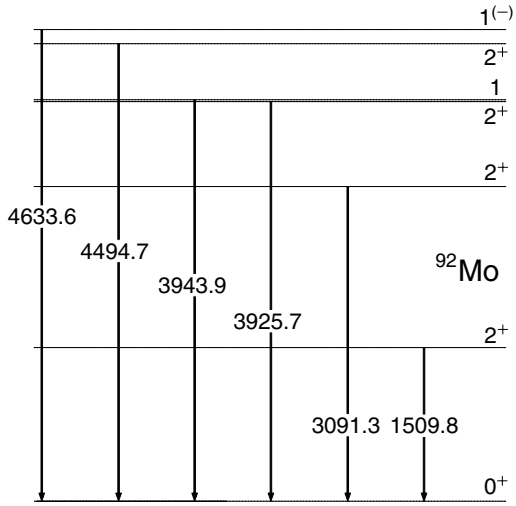

FIG. 3. Level scheme of ^{92}Mo deduced from the present photon-scattering experiment at $E_e = 6$ MeV. Parities of the levels were taken from Ref. [33].

B. Photon-scattering experiments on ^{98}Mo

The nuclide ^{98}Mo was studied in photon-scattering experiments at the Dynamitron accelerator of the University of Stuttgart. The measurements were carried out at electron energies of $E_e = 3.3$ and 3.8 MeV. The average electron current was 250 μA. The electron beam was completely stopped in a 4 mm thick gold radiator, thus producing bremsstrahlung. The collimated photon beam irradiated the targets placed in an evacuated photon-beam pipe. The target of ^{98}Mo with a mass of 1998 mg and an enrichment of 98.55% was combined with 757 mg of ^{27}Al used for the calibration of the photon flux. A sample of isotopically enriched ^{13}C with a mass of 102 mg was additionally used in the measurement at 3.8 MeV. The relative photon flux determined from transitions in ^{27}Al was interpolated by using the formula given in Ref. [35]. γ rays scattered from the target were measured with three HPGe detectors placed at 90°, 127°, and 150°, relative to the incident photon beam and at distances of 20 cm from the target. The detectors had relative efficiencies of 100% and were shielded with lead against background radiation. In addition, the detector at 127° was surrounded by an escape-suppression shield consisting of BGO scintillation detectors. Spectra of scattered photons were measured for 90 h in the experiment at $E_e = 3.8$ MeV and for 60 h in the experiment at $E_e = 3.3$ MeV. Parts of spectra measured at 150° for $E_e = 3.3$ and $E_e = 3.8$ MeV are shown in Fig. 4.

Six transitions were observed in ^{98}Mo for the first time and are given in Table I. The angular distributions of the newly observed transitions shown in Fig. 5 indicate dipole character. Their partial widths are clearly above the detection limits (see Fig. 5). The comparison of the spectra measured at different electron energies (cf. Fig. 4) reveals that the transition at 2816.9 keV is observed at $E_e = 3.8$ MeV, but not at $E_e = 3.3$ MeV. Based on the transition strength deduced for the 2816.9 keV transition from the spectrum at $E_e = 3.8$ MeV, this transition should have been observed in the spectrum at

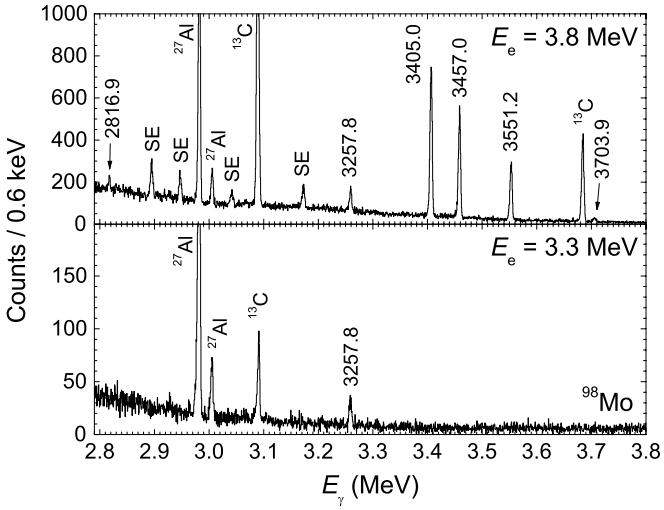

FIG. 4. Spectra of photons scattered from ^{98}Mo at 150° relative to the beam at electron energies of 3.8 MeV (top) and 3.3 MeV (bottom). Peaks labeled with their energies in keV correspond to transitions assigned to ^{98}Mo. SE marks single-escape peaks.

$E_e = 3.3$ MeV as a peak containing about 200 counts (cf. Fig. 4), i.e., eight times more than the detection limit (see open circle in Fig. 5), if it was a ground-state transition. This means that the 2816.9 keV transition deexcites a state at an energy greater than 3.3 MeV. Indeed, the transition at 2816.9 keV fits the energy spacing between the state at 3551.2 keV and the 0_2^+ state at 734.8 keV known from previous work [36]. The level scheme of ^{98}Mo deduced from the present experiments is shown in Fig. 6.

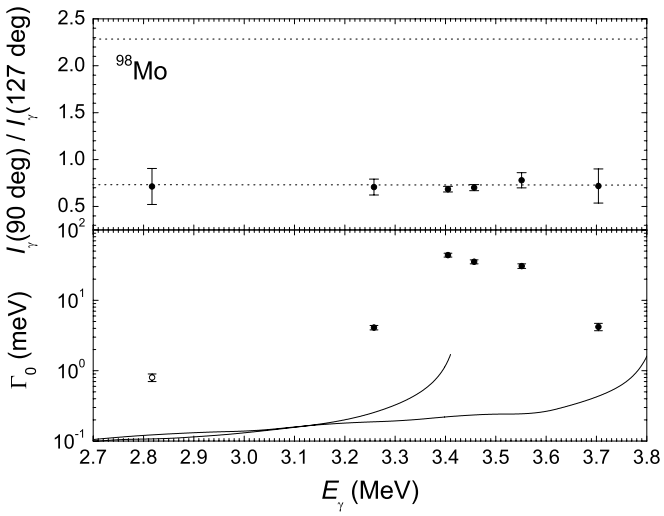

FIG. 5. Top: Ratios $I_\gamma(90°)/I_\gamma(127°)$ for transitions in ^{98}Mo, with the expected values for dipole (0.73) and quadrupole (2.28) transitions shown as dotted lines. Bottom: Partial widths of ground-state transitions (filled circles) and a branching transition (open circle), see text, with the detection limits obtained from the measured spectra at 150° and at electron energies of 3.8 and 3.3 MeV (solid lines).

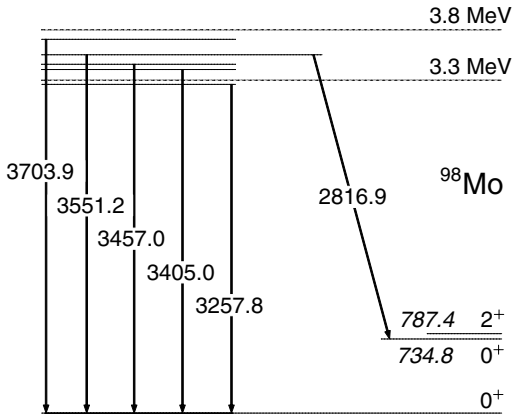

FIG. 6. Level scheme of ^{98}Mo including the $J = 1$ states found in the present work (left) and known low-lying states [36](right). The used electron energies are indicated by dashed lines.

C. Photon-scattering experiments on ^{100}Mo

Excited levels in ^{100}Mo were populated via (γ, γ') reactions up to 3.8 MeV. Three experiments were carried out at the Dynamitron accelerator at electron energies of 3.2, 3.4, and 3.8 MeV and an average electron current of 250 μA. A sample of ^{100}Mo with a mass of 1620 mg, isotopically enriched to 99.00%, was used as a target. The target was combined with ^{27}Al and ^{13}C samples with masses of 757 mg and 102 mg, respectively, for photon-flux calibration. The detector setup was the same as in the ^{98}Mo experiments. Parts of γ-ray spectra measured at 150° are shown in Fig. 7 for $E_e = 3.2$, 3.4, and 3.8 MeV.

At an electron energy of 3.8 MeV, we observed 19 transitions for the first time, which are given in Table I. The ratios $I_\gamma(E_\gamma, 90°)/I_\gamma(E_\gamma, 127°)$ shown in Fig. 8 indicate dipole character for all transitions. The comparison of the spectra measured at different electron energies allowed us to distinguish between ground-state transitions and transitions populating low-lying levels as described above for ^{98}Mo. In the following paragraphs the determination of the branching transitions is described in detail.

The 3290.1 keV level. The transitions at 2595.2 and 2754.7 keV fit the energy spacings between this level and the 0_2^+ state at 695.1 keV and the 2_1^+ state at 535.6 keV, respectively, known from previous work [37]. These transitions were not observed in the measurement at $E_e = 3.2$ MeV (cf. Fig. 7). If the transitions at 2595.2 and 2754.7 keV were ground-state transitions, they should have occurred in the spectrum at $E_e = 3.2$ MeV as peaks with areas of about 140 and 330 counts, respectively, which is 8 and 12 times more than the respective detection limits (cf. Fig. 8). Therefore, we consider them as branches from the 3290.1 keV level to the 0_2^+ and 2_1^+ states. On the basis of the Alaga rules [cf. Eq. (3)], we propose positive parity for this state.

The 3483.4 keV level. The transitions at 2948.2 and 2419.8 keV are observed in neither the measurement at $E_e = 3.4$ MeV nor the one at $E_e = 3.2$ MeV. Assuming that these transitions are ground-state transitions and using the scattering cross section determined from the spectrum at

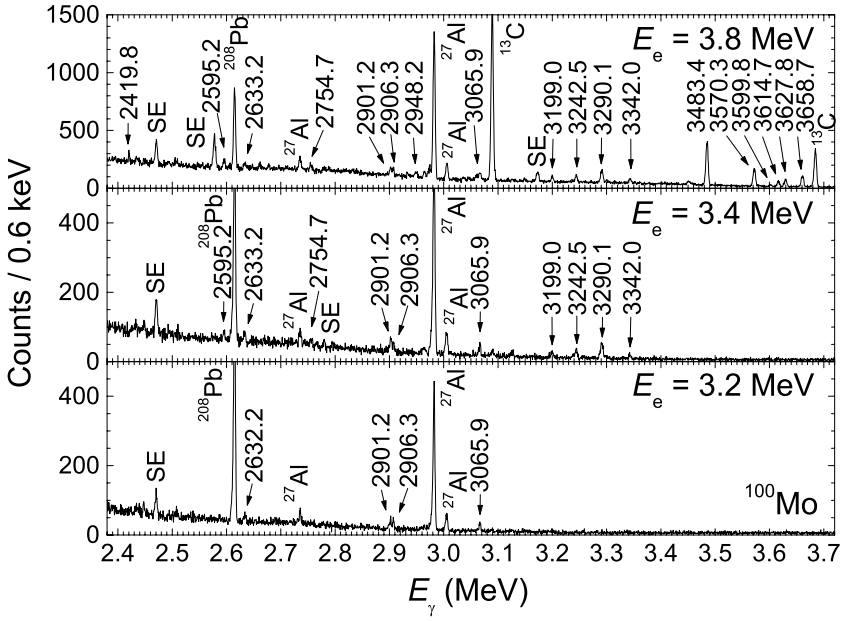

FIG. 7. Photon spectra from ^{100}Mo, measured at 150° relative to the beam and at three electron energies. Peaks labeled with their energies in keV correspond to dipole transitions assigned to ^{100}Mo. SE marks single-escape peaks.

$E_e = 3.8$ MeV, they should occur in the spectra measured at $E_e = 3.2$ MeV as peaks with areas of 190 and 240 counts, respectively, and at $E_e = 3.4$ MeV as peaks with 350 and 340 counts, respectively, which is not the case. These areas are 6 and 10 times higher than the respective detection limits for the spectrum at $E_e = 3.2$ MeV, and 8 and 15 times higher than the respective detection limits in the spectrum at $E_e = 3.4$ MeV. As the 2948.2 and 2419.8 keV transitions fit the respective energy spacings between the 3483.4 keV level and the 2_1^+ and 2_2^+ states, they are assigned as branches to these states. Based on the Alaga rules, we assign tentatively positive parity to this state.

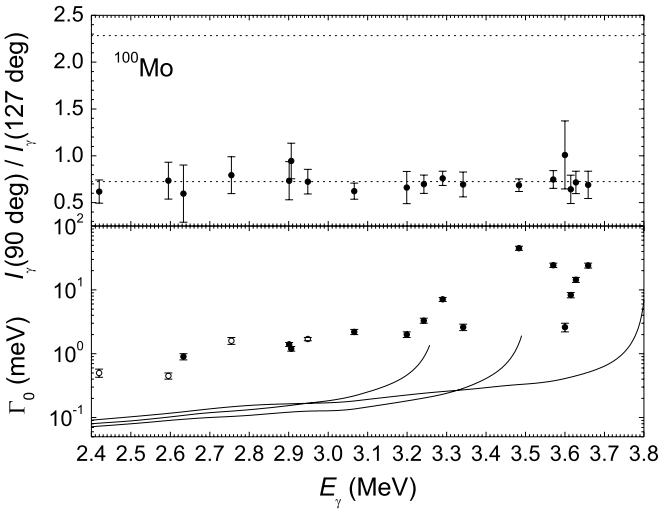

FIG. 8. Top: Ratios of γ-ray intensities observed at 90° and 127° relative to the beam. Expected values for pure dipole (0.73) and quadrupole (2.28) transitions in even-even nuclei are shown as dotted lines. Bottom: Partial widths Γ_0 of ground-state transitions (filled circles) and branching transitions (open circles), with the detection limits obtained from the spectra measured at 150° and $E_e = 3.2$, 3.4, and 3.8 MeV (solid lines).

The 3658.8 keV level. The transition at 2595.2 keV fits the energy spacing between this level and the 2_2^+ state. However, it was also assigned as a branch from the level at 3290.1 keV to the 0_2^+ state. In the measurement at $E_e = 3.8$ MeV, the peak at 2595.2 keV is observed with about twice the intensity observed at $E_e = 3.4$ MeV, where the level at 3658.8 keV is not excited. This proves that the two transitions depopulating the 3290.1 and 3658.8 keV levels, exist with nearly equal intensities. Thus, the 2595.2 keV transition is also assigned as populating the 3658.8 keV level to the 2_2^+ state. Positive parity is tentatively assigned to this state on the basis of the Alaga rules.

The level scheme of ^{100}Mo deduced from the present experiments is shown in Fig. 9.

III. SYSTEMATICS OF *M*1 STRENGTH

In the following we will discuss the systematic behavior of the $M1$ strength in the chain of even-mass Mo isotopes

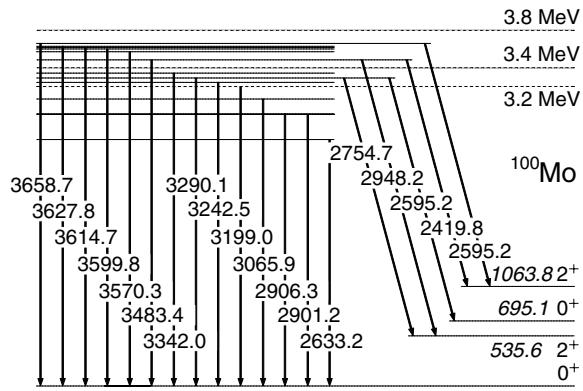

FIG. 9. Level scheme of ^{100}Mo including the $J = 1$ states found in the present work (left) and known low-lying states (right) [37]. Electron energies used are indicated by dashed lines.

from ^{92}Mo ($N = 50$) to ^{100}Mo ($N = 58$) in comparison with predictions of the standard quasiparticle random-phase approximation (QRPA) [38,39] and, the shell model. The results of the present experiments are complemented by the ones of previous work on ^{94}Mo [13,14] and ^{96}Mo [16]. In ^{94}Mo and ^{96}Mo, also, one and two 1^- states, respectively, were identified, which are considered as the 1^- members of the $2^+ \otimes 3^-$ quintuplet and include about 13% and 30%, respectively, of the total dipole strength in the considered energy region [14,16]. In the following discussion we assume positive parity for all $J = 1$ states up to 4 MeV in ^{98}Mo and ^{100}Mo, but keep in mind that a few of the observed states may have negative parity. The cumulative $M1$ strengths in the chain of Mo isotopes are presented in Fig. 10.

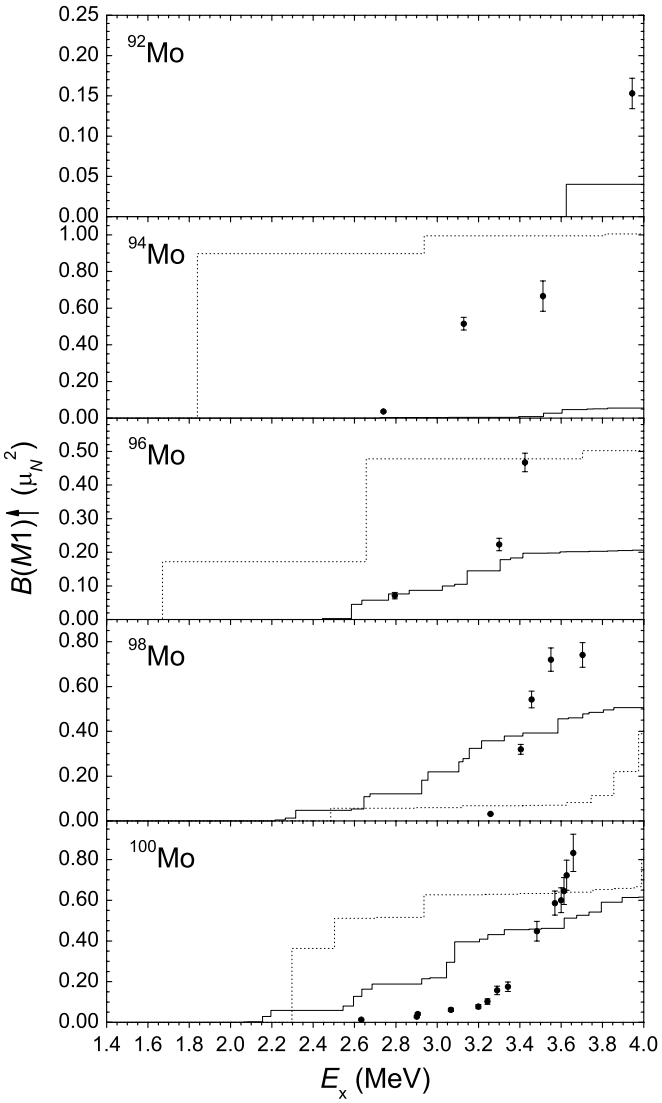

FIG. 10. Cumulative $M1$ strengths in the stable even-mass Mo isotopes. Experimental values are given as filled circles. Results of QRPA and shell-model calculations are shown as solid and dotted lines, respectively. Note that the experimental values for ^{98}Mo and ^{100}Mo are based on the assumption of positive parity for all $J = 1$ states observed in the present experiments (cf. Table I).

TABLE II. Deformation parameters of the ground states and summed $M1$ strengths up to 4 MeV for the even-even Mo isotopes.

A	ε_2	γ	$\sum B(M1) \uparrow / \mu_N^2$		
			Exp[a]	SM[b]	QRPA[c]
92	0.0	–	0.15(2)	–	0.06
94	0.02	–	0.67(7)	1.01	0.06
96	0.10	60°	0.47(2)	0.50	0.19
98	0.18	37°	0.74(6)	0.39	0.45
100	0.21	32°	0.83(9)	0.81	0.54

[a]Experimental values.
[b]Shell-model calculations.
[c]QRPA calculations.

A. QRPA calculations

The structure of the ground states is known to change from a spherical shape at $A = 92$ to a deformed one at $A = 100$ (cf. Ref. [40]) which is expected to influence the strength distribution of the dipole excitations in the Mo isotopic chain with $A = 92$–100. As a necessary ingredient of the QRPA calculations, the equilibrium shapes of the ground states were determined by using the Nilsson-Strutinsky method [41] including pairing properties with the gap parameters given in Ref. [42]. The resulting potential energy surfaces (PES) are shown in Fig. 11. They reflect the shape change from the nearly spherical nuclei ^{92,94}Mo to relatively soft PES with triaxial minima in ^{98,100}Mo. The deformation parameters of the minima are given in Table II.

Before discussing the results of the calculations, we would like to mention that the exact location and strength of the dipole transitions cannot be predicted in detail, because for deformed nuclei an advanced QRPA code, in which all input quantities could be calculated fully self-consistently with realistic residual interactions, was hitherto not available. Thus, in order to make the QRPA approach applicable for deformed nuclei, we used the empirical Nilsson model and phenomenological residual interactions. Another problem is that in the standard QRPA aiming at the calculation of dipole states, the coupling with states of other multipolarities is neglected. These missing couplings lead to shifts of the states and redistributions of the strengths. Their approximate treatment in terms of a phonon-phonon approach [39,43] may improve the description, but in detail the discrepancy to the individual data remains. In spite of the above simplifications, the QRPA is the appropriate tool for describing the gross features of $M1$ strength distributions such as the summed strength and its dependence on nucleon numbers and on the shapes of the nuclei. We are going to discuss the following questions:

(i) Is the QRPA, which includes the deformation change in the series $A = 92$–100, able to describe the observed *summed* dipole strength in the energy range of $E \approx 2.5$–4 MeV and what $M1$ strength is predicted at higher energy?
(ii) What can be learned about the structure of the excitation modes and the residual interaction?

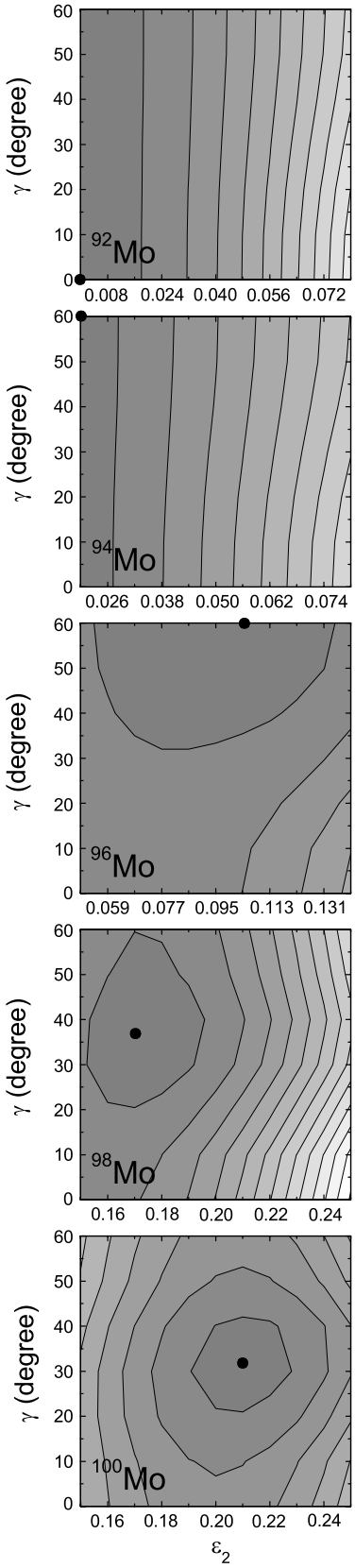

FIG. 11. Potential energy surfaces as functions of the deformation parameters ε_2 and γ for the even-even Mo isotopes. Minima are marked with black circles. The difference between the contour lines is 0.08 MeV.

Our QRPA calculations use a mixture of separable multipole-multipole residual interactions with the strength parameters described below. As a helpful tool for analyzing the calculated QRPA spectra, the method of mode suppression [44] is applied which enables the complete elimination of spurious modes and, moreover, can be used to characterize the types of excitations in terms of the different interactions.

Firstly, we calculated the excitation energies and $E1$ transition strengths of $J^\pi = 1^-$ states using the QRPA with doubly stretched coordinates [45]. The strength parameters of the isovector dipole-plus-octupole interaction implemented in the QRPA for the 1^- states has been fixed by the self-consistency conditions [45] together with the known position of the giant $E1$ resonance. In the considered energy region, the QRPA calculations yield a summed $E1$ strength smaller than $10^{-5}\, e^2\,\mathrm{fm}^2$, which is below the detection limit of our experiments. Because the QRPA gives practically no strength to the electric-dipole states below 4 MeV, we will restrict the following discussion to $M1$ excitations. States with $J^\pi = 1^-$ in the range up to 4 MeV as found in ^{94}Mo [14] and ^{96}Mo [16] are likely to be two-phonon states formed by a coupling of collective octupole and quadrupole phonons, which are outside the QRPA description. Generally, the QRPA calculations predict substantial $E1$ strength above 6 MeV, which is the average shell gap between the shells of different parities in nuclei around $A = 100$.

The QRPA calculations for the 1^+ excitations shall be described in more detail. The following Hamiltonian was used in the QRPA calculations:

$$H_{M1}^{\mathrm{QRPA}} = h_{\mathrm{MF}} - \frac{1}{2}\sum_{t=0,1}\kappa_j^t \mathbf{J}^t\cdot\mathbf{J}^t - \frac{1}{2}\sum_{t=0,1}\kappa_s^t \mathbf{S}^t\cdot\mathbf{S}^t. \quad (8)$$

The term h_{MF} in Eq. (8) includes the Nilsson mean field plus monopole pairing using the equilibrium deformation derived before. The following terms $\mathbf{J}^t\cdot\mathbf{J}^t$ (jj) and $\mathbf{S}^t\cdot\mathbf{S}^t$ (ss) are interaction terms composed of the isoscalar $(t = 0)$ and isovector $(t = 1)$ parts of the total angular momentum operator $\mathbf{J} = \mathbf{L} + \mathbf{S}$ and the spin operator $\mathbf{S}$, i.e., $\mathbf{J}^{t=0,1} = \mathbf{J}^\pi + (-1)^t\mathbf{J}^\nu$ and $\mathbf{S}^{t=0,1} = \mathbf{S}^\pi + (-1)^t\mathbf{S}^\nu$, where π and ν stand for proton and neutron, respectively. The actual strength of the interaction terms is tuned by the values of the parameters κ_j^t and κ_s^t in Eq. (8). A quadrupole-quadrupole interaction term turned out to be not important for the dipole states under study.

We now explain briefly the essence of the suppression method [44] for the removal of the spurious oscillations of the total angular momentum $\mathbf{J}$ considered below. The quadratic term $\kappa_j\mathbf{J}\cdot\mathbf{J}$ in the QRPA Hamiltonian (8) acts as an oscillator spring force for the angular momentum $\mathbf{J}$ with the tunable stiffness parameter κ_j. Hence, by choosing the stiffness parameter κ_j to be rather large, the frequency of the unwanted oscillations of $\mathbf{J}$ contributing to the QRPA spectrum can be shifted up to any high energy such that this spurious motion becomes frozen, i.e., this mode gets too "hard" to be excited within the considered energy range. With the same method, the oscillatory motion of any other selected operator can be eliminated. This technique is used to analyze the structure of the phonon excitations.

The $M1$ transition operator can be expressed by the same operators $\mathbf{J}^t$ and $\mathbf{S}^t$ determining the interaction terms in Eq. (8):

$$\widehat{\mathbf{M1}} = \sqrt{\frac{3}{4\pi}}(\mathbf{L}^\pi + g_s^\pi \mathbf{S}^\pi + g_s^\nu \mathbf{S}^\nu) = \sqrt{\frac{3}{4\pi}}\left(\frac{1}{2}\mathbf{J}^{t=0} + \frac{1}{2}\mathbf{J}^{t=1} + g_s^{t=0}\mathbf{S}^{t=0} + g_s^{t=1}\mathbf{S}^{t=1}\right). \quad (9)$$

With the usual gyromagnetic factors g_s^π and g_s^ν and an attenuation factor of 0.7, one obtains the values $g_s^{t=0} = 0.12\,\mu_N$ and $g_s^{t=1} = 2.79\,\mu_N$ for the strengths of the isoscalar- and isovector-spin parts, respectively, of the $M1$ transition operator. From the decomposition (9), the following general conclusions can be drawn for the $M1$ transition matrix elements. The term proportional to the total angular momentum ($\sim\mathbf{J}^{t=0} \equiv \mathbf{J}$) should not contribute at all, since for an exact calculation the relation $\langle 1^+|\mathbf{J}|0\rangle = 0$ holds automatically. However, the QRPA for the deformed case does not satisfy angular-momentum conservation. Therefore, it is a necessary requirement for an accurate QRPA treatment of deformed nuclei to make sure that the transition amplitudes $\langle ph|\mathbf{J}|0\rangle$ vanish for all phonon excitations $|ph\rangle$ to the QRPA ground state $|0\rangle$. This is achieved by the suppression of the spurious motion from $\mathbf{J}$. The isovector-orbital term ($\sim\mathbf{J}^{t=1} = \mathbf{J}^\pi - \mathbf{J}^\nu$) is known to generate proton-neutron contrarotational 1^+ states [5] which, in principle, can attract a large part of the available $M1$ strength below 5 MeV [7]. Such an isovector-jj contribution is expected to be large when high-j proton and neutron orbits get excited because of their sizable angular-momentum content. The isoscalar-spin contribution ($\sim\mathbf{S}^{t=0}$) is strongly quenched by the factor of 0.12, whereas the isovector-spin contribution ($\sim\mathbf{S}^{t=1}$) is the largely favored term because of the factor of 2.79. Hence, the total $M1$ transition strength is determined practically from only the isovector-jj term and the isovector-ss terms. The particular distribution of the $M1$ strength on the energy (i.e., the spectral distribution) depends, of course, also on the occupation and quantum numbers of the deformed orbits involved in the QRPA phonon excitations. As mentioned above, the QRPA calculations started with the elimination of the spurious angular-momentum contributions. For this purpose, the isoscalar-jj interaction term is taken with a sufficiently large strength of $\kappa_j^{t=0} \geqslant 10^2$ MeV/$\hbar^2$, which is strong enough to achieve $\langle ph|\mathbf{J}|0\rangle = 0$ [44] for all resulting QRPA phonon states.

For the spin-spin interaction, there is no unique choice for the isoscalar and isovector strength parameters to be directly applied. The compilation given in Ref. [46] offers a whole set of values used in the literature. Since the $M1$ strength is not sensitive against the isoscalar-ss interaction, we have chosen $\kappa_s^{t=0} = 0$. The constant $\kappa_s^{t=1} = -1$ MeV/$\hbar^2$ taken for the repulsive isovector-ss interaction is a favorable value to move the main part of the spin-magnetic strength to about 8 MeV, which is the suggested energy region of the isovector-spin contribution [2,3].

Contrary to the ss interaction, the isovector-jj term in Eq. (8) cannot be derived from an effective two-body interaction. Therefore, this term was exclusively used to analyze the $M1$ strength with respect to the isovector-orbital contribution. Using a large value $\kappa_j^{t=1} \geqslant 10^2$ MeV/$\hbar^2$ for the isovector-jj term, we get $\langle ph|\mathbf{J}^{t=0}|0\rangle = 0$, i.e., the contribution of this mode to the calculated $M1$ strength is suppressed. The comparison of the result with the transition strength without such a suppression allows us to estimate the contribution of the isovector-orbital mode. As expected, there is practically no such contribution to the low-lying $M1$ strength for the nearly spherical cases ^{92,94,96}Mo, whereas in the deformed isotopes ^{98}Mo and ^{100}Mo the isovector-orbital mode exhausts 53% and 56%, respectively, of the summed $M1$ strength. Similarly, the contributions from the isovector-spin amplitudes $\langle ph|\mathbf{S}^{t=0,1}|0\rangle$ to the $M1$ strength were determined by choosing large values of $\kappa_s^{t=1} \geqslant 10^2$ MeV/$\hbar^2$, such that this contribution is suppressed.

B. Shell-model calculations

Shell-model calculations were performed using a model space including the active proton orbits $\pi(0f_{5/2}, 1p_{3/2}, 1p_{1/2}, 0g_{9/2})$ and neutron orbits $\nu(0g_{9/2}, 1d_{5/2}, 0g_{7/2})$ relative to a hypothetical ^{68}Ni core. Since an empirical set of effective interactions for this model space is not available as yet, various empirical interactions have been combined with results of schematic nuclear interactions applying the surface delta interaction. Details of this procedure are described in Refs. [47,48]. The single-particle energies relative to the ^{68}Ni core have been derived from the single-particle energies of the proton orbits given in Ref. [49] with respect to the ^{78}Ni core and from the neutron single-hole energies of the $0g_{9/2}, 0g_{7/2}$ orbits [50]. The transformation of these single-particle energies to those relative to the ^{68}Ni core has been performed [51] on the basis of the effective residual interactions given in, e.g., Refs. [47,48]. The obtained values are $\epsilon^\pi_{0f_{5/2}} = -9.806$, $\epsilon^\pi_{1p_{3/2}} = -9.733$, $\epsilon^\pi_{1p_{1/2}} = -7.427$, $\epsilon^\pi_{0g_{9/2}} = -1.227$, $\epsilon^\nu_{0g_{9/2}} = -6.582$, $\epsilon^\nu_{1d_{5/2}} = -4.395$, and $\epsilon^\nu_{0g_{7/2}} = -0.623$ MeV. $M1$ transition strengths were calculated with effective g factors of $g_s^{\rm eff} = 0.7 g_s^{\rm free}$. To make the calculations feasible, a truncation of the occupation numbers was applied. Two protons were allowed to be lifted from the $1p_{1/2}$ orbit to the $0g_{9/2}$ orbit. One $0g_{9/2}$ neutron could be lifted over the shell gap either to the $1d_{5/2}$ or to the $0g_{7/2}$ orbit. For ^{98}Mo and ^{100}Mo, a maximum of two neutrons could be excited from the $1d_{5/2}$ to the $0g_{7/2}$ orbit. With these restrictions, configuration spaces with dimensions of up to 3000 were obtained for the 1^+ states. The calculations were carried out with the code RITSSCHIL [53].

C. Comparison of experimental and calculated $M1$ strengths

The cumulative $M1$ strengths versus the excitation energy obtained from the shell-model and QRPA calculations are shown in Fig. 10 together with the experimental values. There is no one-to-one correspondence between the calculated and experimental $M1$ strength distributions.

The shell-model calculations predict an increase in the number of 1^+ states with increasing neutron number above the $N = 50$ shell closure. While there is no 1^+ state in the

considered energy range up to 4 MeV in ^{92}Mo, there are three 1^+ states in ^{94}Mo and ^{96}Mo, 10 in ^{98}Mo and 12 in ^{100}Mo. The summed $M1$ strengths predicted by the shell-model calculations are shown in Fig. 12 and Table II. The large summed strength in ^{94}Mo is dominated by one state with the main configuration $\pi(0g_{9/2}^2)\nu(1d_{5/2}^2)$, which has a calculated strength of $B(M1, 0^+ \rightarrow 1^+) = 0.90\,\mu_N^2$. This special four-particle configuration corresponds to a two-phonon state, which cannot be described in the QRPA calculations. The calculated summed $M1$ strengths in ^{96}Mo and ^{100}Mo agree with the experimental values, while the value predicted for ^{98}Mo is too small. The calculated summed strength in ^{100}Mo is dominated by the value of $B(M1, 0^+ \rightarrow 1^+) = 0.36\,\mu_N^2$ of a state with the four-particle configuration $\pi(0g_{9/2}^2)\nu(0g_{7/2}^2)$ that is analogous to the case of ^{94}Mo.

The QRPA calculations reproduce the fact that the $M1$ strength is distributed over only a few states in the spherical nuclei ^{92,94}Mo, while there are many states with smaller individual $B(M1)$ values in the deformed nuclei ^{98,100}Mo (cf. Fig. 10). This tendency of an increasing spread of the strength is a direct consequence of the increasing splitting of the orbit energies with increasing deformation. As shown in Fig. 12 and Table II, the summed $M1$ strengths obtained from the QRPA calculations underestimate the experimental ones. However, the increase of the summed $M1$ strengths with increasing neutron number is reproduced. The discrepancy between the calculated and experimental summed $M1$ strengths in ^{94}Mo is caused by the fact that the dominant $M1$ strength is generated by a special four-particle configuration (see above). Summarizing, the results of the QRPA calculations show that deformation causes a spread of the $M1$ strength distribution and an increase in the summed $M1$ strength. The spread is a direct consequence of the energetic spread of the quasiparticle states for a deformed system. As a result of the QRPA calculations, we found the $M1$ strengths in the nearly spherical nuclei to be generated by isovector-spin vibrations only while the $M1$ strengths in the deformed nuclei are a combination of isovector-orbital vibrations and isovector-spin vibrations. A pure isovector-orbital character of the 1^+ excitations is absent possibly because there are no proton and neutron deformation-aligned high-j orbits in the Mo isotopes with $A = 92$–100, which create the favored situation for the isovector angle rotation.

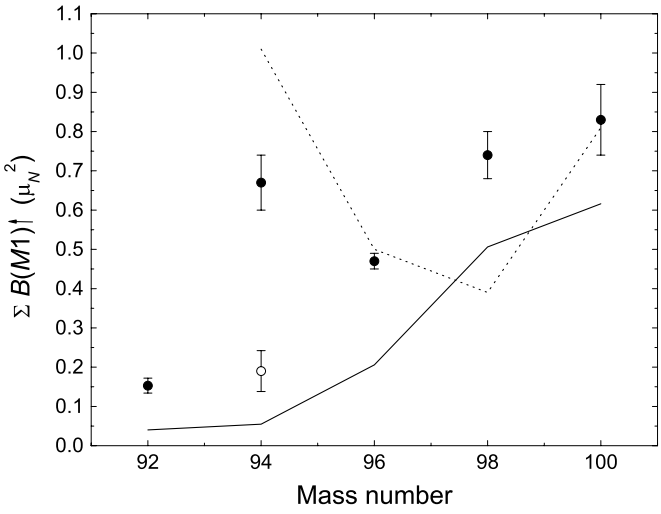

FIG. 12. Comparison of the experimental summed $M1$ strengths up to 4 MeV (filled circles) with predictions of QRPA calculations (solid line) and shell-model calculations (dotted line). Contribution of the mixed-symmetry state in ^{94}Mo, which is not described in the QRPA calculations, to the experimental summed $M1$ strength is $0.48(3)\,\mu_N^2$ [14]. Open circle represents the value without this contribution.

D. $M1$ strength predicted at high energy

In addition to the energy range covered by the present experiments, we performed QRPA calculations up to an excitation energy of 10 MeV. The predicted $M1$ strength distributions are shown in Fig. 13. The summed $M1$ strengths in this extended energy range reach values of $\sum B(M1)\uparrow \approx 3$–$4\,\mu_N^2$, which is the maximum expected from particle-hole excitations for the $N = 3$, 4 shell. In the QRPA calculations, it turns out that practically all the transition strength of the isovector-orbital type ($\approx 0.5\,\mu_N^2$ in the deformed nuclei) is concentrated below 4 MeV excitation energy, while the bump of $M1$ transitions predicted above 4 MeV with a large summed strength of about $\sum B(M1) \approx 3\,\mu_N^2$ is exclusively caused by isovector-spin vibrations. The contributions of isovector-orbital vibrations to the total $M1$ strengths in the spherical ^{92}Mo and deformed

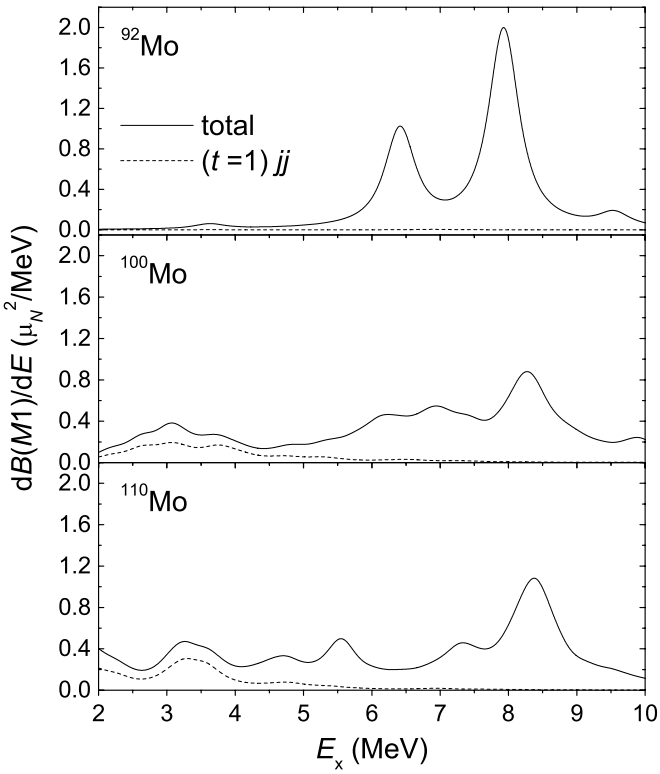

FIG. 13. Contributions of different types of vibrations to the $M1$ strength distributions in ^{92}Mo (top), ^{100}Mo, and ^{110}Mo. Solid lines represent the total strengths; dashed lines show the isovector-orbital contributions.

^{100}Mo are depicted in Fig. 13. In addition, the $M1$ strength predicted for the neutron-rich isotope ^{110}Mo is plotted. The equilibrium deformation parameters obtained for this nuclide are $\varepsilon_2 = 0.23$ and $\gamma = 60^\circ$.

Shell-model calculations carried out for the spherical ^{92}Mo up to about 8.5 MeV predict a 1^+ state with a large strength of $B(M1)\uparrow = 4.8\,\mu_N^2$ at 8.2 MeV which is dominated by the spin-flip configuration $\nu(0g_{9/2}^{-1}0g_{7/2}^{1})$.

IV. CONCLUSIONS

The nuclides ^{92}Mo, ^{98}Mo, and ^{100}Mo were investigated in photon-scattering experiments with bremsstrahlung. Various electron-beam energies were used in order to resolve branching transitions in ^{98}Mo and ^{100}Mo. Five $J = 1$ states up to $E_x = 4$ MeV in ^{98}Mo and 14 in ^{100}Mo were observed for the first time. The transition strengths deduced from the present experiments for ^{92}Mo, ^{98}Mo, and ^{100}Mo together with known values for ^{94}Mo and ^{96}Mo allowed us to study the systematics of the low-lying magnetic dipole excitations in the chain of stable even-even Mo isotopes.

The experimental results are compared with predictions of QRPA calculations in a deformed basis and with predictions of the shell model. The QRPA calculations reproduce the growth and spread of the $M1$ strength with increasing neutron number. The substantial $M1$ strength observed in the deformed isotopes ^{98}Mo and ^{100}Mo can be explained in the QRPA calculations by a combination of the isovector-spin and isovector-orbital vibrations. The shell-model calculations especially reproduce the large $M1$ strength in ^{94}Mo as caused by a special four-particle configuration that is outside the scope of the QRPA. The appearance of a broad bump of strong $M1$ excitations predicted in the QRPA calculations for excitation energies of 5–9 MeV may be reviewed in future measurements which determine the parities of dipole excitations in this energy region.

For the neighboring nucleus ^{90}Zr, electron-scattering data [53] show a summed $M1$ strength of $\sum B(M1, 0^+ \rightarrow 1^+) = 0.8\,\mu_N^2$ around an excitation energy of 8 MeV. The analysis of data from polarized-photon scattering [54] indicates that additional strength of several μ_N^2 is hidden in the continuum between strong $E1$ transitions. Assuming a summed $M1$ strength of about $3\,\mu_N^2$ at 7–8 MeV as resulting from our calculations, we derive an average photon absorption cross section of 1 mb. Even for the exotic Mo isotopes with $A \leqslant 90$ ($A \geqslant 106$), for which the proton (neutron) separation energies are less than 7 MeV, the $M1$ cross sections do not determine the photodissociation process, which is of importance in hot cosmic scenarios. As estimated in Ref. [55], the $E1$ absorption cross section just above the particle-separation energy is larger than the $M1$ absorption cross section by about one order of magnitude in these nuclides.

ACKNOWLEDGMENTS

This work was supported by the Deutsche Forschungsgemeinschaft under contracts Do-466/1-2 and Kn-154/31. L.K.K. and G.R. acknowledge support by the Bulgarian NRF under Contract PH 908. S.F. is supported by the DOE with Grant No. DE-FG02-95ER40934.

[1] A. Bohr and B. R. Mottelson, in *Nuclear Structure* (Benjamin, New York, 1975), Vol. 2, Ch. 5.
[2] D. Zawischa, M. Macfarlane, and J. Speth, Phys. Rev. C **42**, 1461 (1990).
[3] P. Sarriguren, E. Moya de Guerra, R. Nojarov, and A. Faessler, J. Phys. G **19**, 291 (1993).
[4] W. Knüpfer, M. Dillig, and A. Richter, Phys. Lett. **B95**, 349 (1980).
[5] N. Lo Iudice and F. Palumbo, Phys. Rev. Lett. **41**, 1532 (1978).
[6] D. Bohle, A. Richter, W. Steffen, A. E. L. Dieperink, N. Lo Iudice, F. Palumbo, and O. Scholten, Phys. Lett. **B137**, 27 (1984).
[7] A. Richter, Prog. Part. Nucl. Phys. **34**, 261 (1995).
[8] U. Kneissl, H. H. Pitz, and A. Zilges, Prog. Part. Nucl. Phys. **37**, 349 (1996).
[9] W. Ziegler, C. Rangacharyulu, A. Richter, and C. Spieler, Phys. Rev. Lett. **65**, 2515 (1990).
[10] J. Margraf, R. D. Heil, U. Kneissl, U. Maier, H. H. Pitz, H. Friedrichs, S. Lindenstruth, B. Schlitt, C. Wesselborg, P. von Brentano, R. D. Herzberg, and A. Zilges, Phys. Rev. C **47**, 1474 (1993).
[11] N. Lo Iudice and A. Richter, Phys. Lett. **B304**, 193 (1993).
[12] I. Hamamoto and S. Aberg, Phys. Lett. **B145**, 163 (1984).
[13] N. Pietralla, C. Fransen, D. Belic, P. von Brentano, C. Frießner, U. Kneissl, A. Linnemann, A. Nord, H. H. Pitz, T. Otsuka, I. Schneider, V. Werner, and I. Wiedenhöver, Phys. Rev. Lett. **83**, 1303 (1999).
[14] C. Fransen, N. Pietralla, Z. Ammar, D. Bandyopadhyay, N. Boukharouba, P. von Brentano, A. Dewald, J. Gableske, A. Gade, J. Jolie, U. Kneissl, S. R. Lesher, A. F. Lisetskiy, M. T. McEllistrem, M. Merrick, H. H. Pitz, N. Warr, V. Werner, and S. W. Yates, Phys. Rev. C **67**, 024307 (2003).
[15] A. F. Lisetskiy, N. Pietralla, C. Fransen, R. V. Jolos, and P. von Brentano, Nucl. Phys. **A677**, 100 (2000).
[16] C. Fransen, N. Pietralla, A. P. Tonchev, M. W. Ahmed, J. Chen, G. Feldman, U. Kneissl, J. Li, V. Litvinenko, B. Perdue, I. V. Pinayev, H. H. Pitz, R. Prior, K. Sabourov, M. Spraker, W. Tornow, H. R. Weller, V. Werner, Y. K. Wu, and S. W. Yates, Phys. Rev. C **70**, 044317 (2004).
[17] P. Federman and S. Pittel, Phys. Lett. **B77**, 29 (1978).
[18] P. Federman and S. Pittel, Phys. Rev. C **20**, 820 (1979).
[19] E. Kirchuk, P. Federman, and S. Pittel, Phys. Rev. C **47**, 567 (1993).
[20] M. Zielinska, T. Czosnyka, J. Choinski, J. Iwanicki, P. Napiorkowski, J. Srebrny, Y. Toh, M. Oshima, A. Osa, Y. Utsuno, Y. Hatsukawa, J. Katakura, M. Koizumi, M. Matsuda, T. Shizuma, M. Sugawara, T. Morikawa, H. Kusakari, A. D. Efimov, and V. M. Mikhajlov, Nucl. Phys. **A712**, 3 (2002).
[21] M. Zielinska, T. Czosnyka, K. Wrzosek, J. Choinski, Y. Hatsukawa, J. Iwanicki, M. Koizumi, H. Kusakari,

M. Matsuda, T. Morikawa, P. J. Napiorkowski, A. Osa, M. Oshima, T. Shizuma, J. Srebrny, M. Sugawara, and K. Zajac, Acta Phys. Pol. B **36**, 1289 (2005).
[22] G. Rusev, R. Schwengner, F. Dönau, S. Frauendorf, L. Käubler, L. K. Kostov, S. Mallion, K. D. Schilling, A. Wagner, E. Grosse, H. von Garrel, U. Kneißl, C. Kohstall, M. Kreutz, H. H. Pitz, M. Scheck, F. Stedile, P. von Brentano, J. Jolie, A. Linnemann, N. Pietralla, and V. Werner, Phys. Rev. Lett. **95**, 062501 (2005).
[23] R. Moreh, W. C. Sellyey, and R. Vodhanel, Phys. Rev. C **22**, 1820 (1980).
[24] R. Moreh, O. Beck, I. Bauske, W. Geiger, R. D. Heil, U. Kneissl, J. Margraf, H. Maser, and H. H. Pitz, Phys. Rev. C **48**, 2625 (1993).
[25] N. Pietralla, I. Bauske, O. Beck, P. von Brentano, W. Geiger, R.-D. Herzberg, U. Kneissl, J. Margraf, H. Maser, H. H. Pitz, and A. Zilges, Phys. Rev. C **51**, 1021 (1995).
[26] G. Alaga, K. Alder, A. Bohr, and B. R. Mottelson, Dan. Mat. Fys. Medd. **29**, 9 (1955).
[27] E. Hammaren, P. Heikkinen, K. W. Schmid, and A. Faessler, Nucl. Phys. **A541**, 226 (1992).
[28] A. Zilges, P. von Brentano, H. Friedrichs, R. D. Heil, U. Kneissl, S. Lindenstruth, H. H. Pitz, and C. Wesselborg, Z. Phys. A **340**, 155 (1991).
[29] R. Jenkins, R. W. Gould, and D. Gedcke, *Quantitative X-Ray Spectrometry* (Marcel Dekker, New York, 1981).
[30] R. Schwengner, R. Beyer, F. Dönau, E. Grosse, A. Hartmann, A. R. Junghans, S. Mallion, G. Rusev, K. D. Schilling, W. Schulze, and A. Wagner, Nucl. Instrum. Methods Phys. Res. Sec. A **555**, 211 (2005).
[31] G. Roche, C. Ducos, and J. Proriol, Phys. Rev. A **5**, 2403 (1972).
[32] F. R. Metzger, Phys. Rev. C **15**, 2253 (1977).
[33] C. M. Baglin, Nucl. Data Sheets **91**, 423 (2000).
[34] F. Bauwens, Ph.D. thesis, University of Gent, Belgium, 2000 (unpublished).
[35] L. I. Schiff, Phys. Rev. **83**, 252 (1951).
[36] B. Singh and Z. Hu, Nucl. Data Sheets **98**, 335 (2003).
[37] B. Singh, Nucl. Data Sheets **81**, 1 (1997).
[38] P. Ring and P. Schuck, *The Nuclear Many Body Problem* (Springer, New York, 1980).
[39] V. G. Soloviev, A. V. Sushkov, and N. Yu. Shirikova, Phys. Rev. C **56**, 2528 (1997).
[40] P. Möller and J. R. Nix, At. Data Nucl. Data Tables **26**, 165 (1981).
[41] S. G. Nilsson and I. Ragnarsson, *Shapes and Shells in Nuclear Physics* (Cambridge University, Cambridge, 1995).
[42] P. F. Mantica, A. E. Stuchbery, D. E. Groh, J. I. Prisciandaro, and M. P. Robinson, Phys. Rev. C **63**, 034312 (2001).
[43] N. Lo Iudice, A. V. Sushkov, and N. Yu. Shirikova, Phys. Rev. C **64**, 054301 (2001).
[44] F. Dönau, Phys. Rev. Lett. **94**, 092503 (2005).
[45] H. Sakamoto and T. Kishimoto, Nucl. Phys. **A501**, 205 (1989).
[46] A. Faessler and R. Nojarov, Phys. Rev. C **41**, 1243 (1990).
[47] G. Winter, R. Schwengner, J. Reif, H. Prade, L. Funke, R. Wirowski, N. Nicolay, A. Dewald, P. von Brentano, H. Grawe, and R. Schubart, Phys. Rev. C **48**, 1010 (1993).
[48] G. Winter, R. Schwengner, J. Reif, H. Prade, J. Döring, R. Wirowski, N. Nicolay, P. von Brentano, H. Grawe, and R. Schubart, Phys. Rev. C **49**, 2427 (1994).
[49] X. Ji and B. H. Wildenthal, Phys. Rev. C **37**, 1256 (1988).
[50] R. Gross and A. Frenkel, Nucl. Phys. **A267**, 85 (1976).
[51] J. Blomqvist and L. Rydström, Phys. Scr. **31**, 31 (1985).
[52] D. Zwarts, Comput. Phys. Commun. **38**, 365 (1985).
[53] D. Meuer, R. Frey, D. H. H. Hoffmann, A. Richter, E. Spamer, and O. Titze, Nucl. Phys. **A349**, 309 (1980).
[54] R. M. Laszewski, R. Alarcon, and S. D. Hoblit, Phys. Rev. Lett. **59**, 431 (1987).
[55] S. Goriely and E. Khan, Nucl. Phys. **A706**, 217 (2002).